CMOS buried Quad p-n junction photodetector for multi-wavelength analysis

Charles Richard,[1] Thierry Courcier,[1,2,3] Patrick Pittet,[2,3] Stéphane Martel,[4] Luc Ouellet,[4] Guo-Neng Lu,[2,3] Vincent Aimez,[1] and Paul G. Charette,[1,*]

[1]*Université de Sherbrooke, 2500 Boul. de l'Université, Sherbrooke, Québec J1K 2R1, Canada*
[2]*Université de Lyon, F-69622, Lyon, France*
[3]*CNRS, UMR5270, Institut des Nanotechnologies de Lyon, Université Lyon1, Villeurbanne, France*
[4]*Teledyne DALSA Semiconductor, 18 Boul. de l'Aéroport, Bromont, Québec, J2L 1S7, Canada*
[*]*paul.charette@usherbrooke.ca*

Abstract: This paper presents a buried quad p-n junction (BQJ) photodetector fabricated with a HV (high-voltage) CMOS process. Multiple buried junction photodetectors are wavelength-sensitive devices developed for spectral analysis applications where a compact integrated solution is preferred over systems involving bulk optics or a spectrometer due to physical size limitations. The BQJ device presented here is designed for chip-based biochemical analyses using simultaneous fluorescence labeling of multiple analytes such as with advanced labs-on-chip or miniaturized photonics-based biosensors. Modeling and experimental measurements of the spectral response of the device are presented. A matrix-based method for estimating individual spectral components in a compound spectrum is described. The device and analysis method are validated via a test setup using individually modulated LEDs to simulate light from 4-component fluorescence emission.

OCIS codes: (040.5160) Photodetectors; (330.6180) Spectral discrimination; (110.4234) Multispectral and hyperspectral imaging; (170.6280) Spectroscopy, fluorescence and luminescence.

References and links

1. G. N. Lu, M. B. Chouikha, G. Sou, and M. Sedjil, "Colour detection using a buried double p-n junction structure implemented in the CMOS process," Electron. Lett. **32**(6), 594–596 (1996).
2. F. Yang and A. H. Titus, "Integrated colour detectors in 0.18 µm CMOS technology," Electron. Lett. **43**(23), 1279–1281 (2007).
3. K. Liang, W. Li, H. R. Ren, X. L. Liu, W. J. Wang, R. Yang, and D. J. Han, "Color measurement for RGB white LEDs in solid-state lighting using a BDJ photodetector," Displays **30**(3), 107–113 (2009).
4. D. L. Gilblom, S. K. Yoo, and P. Ventura, "Real-time color imaging with a CMOS sensor having stacked photodiodes," Proc. SPIE **5210**, 105–115 (2004).
5. T. Ross, R. K. Henderson, B. Rae, and D. Renshaw, "A buried triple-junction self-reset pixel in a 0.35µm high voltage CMOS process," in *Proceedings of International Image Sensor* Workshop (Cliffhouse Resort Ogunquit, Maine USA, 2007), pp. 279–282.
6. M. Ben Chouikha, G. N. Lu, M. Sedjil, and G. Sou, "Colour detection using buried triple pn junction structure implemented in BiCMOS process," Electron. Lett. **34**(1), 120–122 (1998).
7. R. F. Lyon and P. M. Hubel, "Eyeing the camera: into the next century," in *Proceedings of IS&T/SID 10th Color Imaging* Conference (The Society for Imaging Science and Technology, Scottsdale, Arizona, USA, 2002), pp. 349–355.
8. R. Lansford, G. Bearman, and S. E. Fraser, "Resolution of multiple green fluorescent protein color variants and dyes using two-photon microscopy and imaging spectroscopy," J. Biomed. Opt. **6**(3), 311–318 (2001).
9. H. Tsurui, H. Nishimura, S. Hattori, S. Hirose, K. Okumura, and T. Shirai, "Seven-color fluorescence imaging of tissue samples based on Fourier spectroscopy and singular value decomposition," J. Histochem. Cytochem. **48**(5), 653–662 (2000).
10. C. Richard, A. Renaudin, V. Aimez, and P. G. Charette, "An integrated hybrid interference and absorption filter for fluorescence detection in lab-on-a-chip devices," Lab Chip **9**(10), 1371–1376 (2009).
11. G. N. Lu, "A dual-wavelength method using the BDJ detector and its application to iron concentration measurement," Meas. Sci. Technol. **10**(4), 312–315 (1999).

#155085 - $15.00 USD Received 20 Sep 2011; revised 21 Dec 2011; accepted 4 Jan 2012; published 17 Jan 2012

1. Introduction

Standard CMOS processes allow the fabrication of buried double p-n junction (BDJ) photodetectors for color detection [1–3]. Using the vertical bipolar transistor structure in a BiCMOS process, it is possible to fabricate a buried triple p-n junction (BTJ) detector for trichromatic color detection [4–6]. With recent advances in microfabrication technology, it is now possible to fabricate more complex device structures. In this article, we report on a buried quad p-n junction (BQJ) detector implemented in a HV (high-voltage) CMOS process, having a superior spectral discriminating ability compared to BDJ and BTJ photodetectors.

Multiple buried-junction photodetectors are of high interest in applications requiring spectral analysis but where bulk optics or a spectrometer are undesirable due to physical size limitations, such as for compact imaging devices [7] or miniaturized biochemical analysis systems (labs-on-chip, biosensors, etc.). In fluorescence–based biochemical analyses, for example, systems typically require sets of matched filtering and dichroic optical components to discriminate between the various fluorescence emission bands [8, 9]. In contrast, when coupled to an integrated thin-film excitation blocking filter [10], the BQJ device is capable of quantifying up to 4 separate spectral components unambiguously in a compact chip-based solution. In addition to spectral discrimination, multiple buried-junction photodetectors benefit from increased rejection of noise from source intensity fluctuations, compared to simple photodiodes, because measurements are based on junction current ratios [11].

This article first presents the BQJ device structure followed by the modeled and experimentally-measured spectral responses of the individual junctions. A method for analysing multi-component spectra is described along with criteria for selecting fluorophores that make optimal use of the device characteristics. Finally, experimental validation of the method is presented using LEDs to simulate a multiple-component fluorescence spectrum.

2. Device structure

The BQJ photodetector structure (Fig. 1(a)) was designed and fabricated with the Teledyne DALSA Semiconductor (Bromont, Canada) HVCMOS process. It consists of four stacked buried p-n junctions:

i. shallow p + diffusion / n-base well junction (junction depth: 0.3 µm)

ii. n-base / p-well junction (junction depth: 1.35 µm)

iii. p-well / deep n-well junction (junction depth: 3.5 µm)

iv. deep n-well / p-epi substrate junction (junction depth: 11 µm).

The photodetector has four outputs through the p + diffusion, n-base, p-well and deep n-well contacts, respectively. The p-epi substrate is grounded and the p-n junctions are reversed biased (Fig. 1(b)). The square active area is 200 μm^2 (see Fig. 1(c), showing a circular focused light spot in the middle of the photodetector active area). The simultaneous measurement of the four output currents, I_{oi} (i = 1..4) enables the determination of the junction currents, I_i (i = 1..4):

$$\begin{aligned} |I_1| &= |I_{o1}| \\ |I_2| &= |I_{o2}| - |I_{o1}| \\ |I_3| &= |I_{o3}| - \left(|I_{o2}| - |I_{o1}|\right) \\ |I_4| &= |I_{o4}| - \left(|I_{o3}| - \left(|I_{o2}| - |I_{o1}|\right)\right) \end{aligned} \tag{1}$$

#155085 - $15.00 USD Received 20 Sep 2011; revised 21 Dec 2011; accepted 4 Jan 2012; published 17 Jan 2012

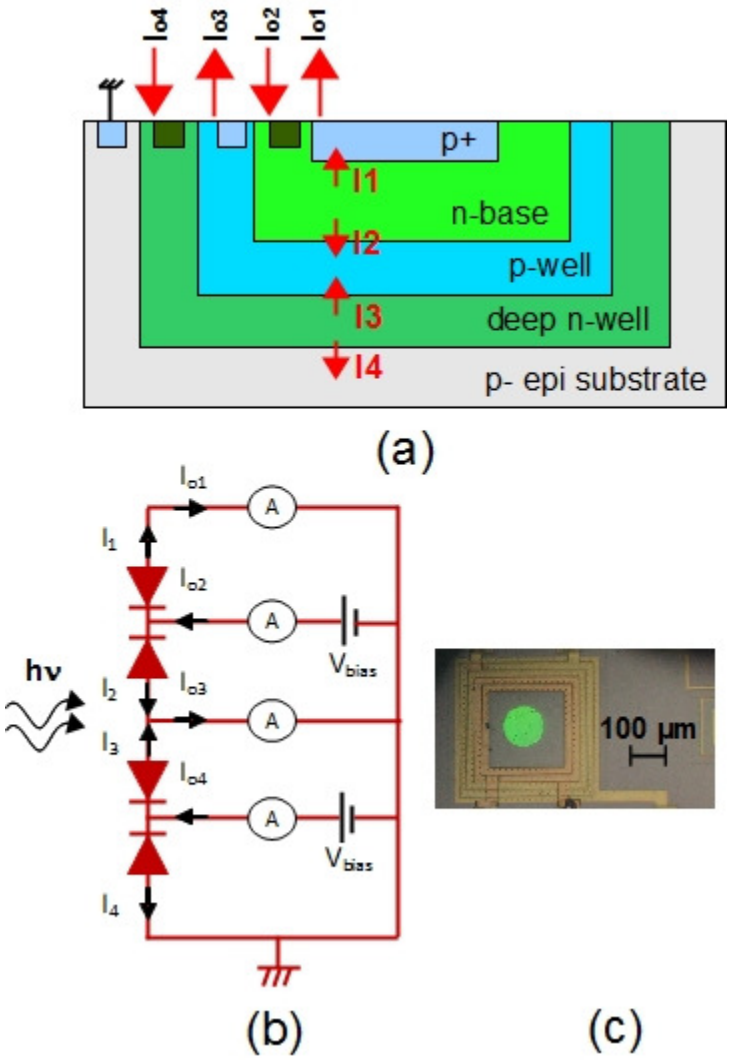

Fig. 1. (a) Schematic representation of the BQJ structure fabricated with the Teledyne DALSA Semiconductor HVCMOS process; (b) Equivalent electrical model with SMU connections (Reverse bias voltage on each junction: −1.5 V); (c) Photograph of the device showing a focused light spot in the middle of the square photodetector active area.

3. Spectral response

The BQJ photodetector structure was modeled with the Taurus Medici semiconductor modeling package (Synopsys Inc., USA). The model was constructed with cylindrical symmetry and included each well of the BQJ structure and the grounded substrate. The spectral response characteristics for each of the four individual junctions were calculated for incident light ranging from 400 nm to 950 nm (Fig. 2). Each junction response has a distinct spectral sensitivity range that is directly related to the junction depth: spectral sensitivity shifts toward longer wavelengths with increasing junction depth.

The actual BQJ spectral responsivity characteristics were determined by illuminating the active surface area of the photodetector with a focused spot of wavelength-swept quasi-monochromatic light generated with a broad-spectrum source (Fiber-Lite High Intensity Illuminator Series 180, Dolan-Jenner Industries Inc., USA) and a tunable optical filter (TOF-

#155085 - $15.00 USD Received 20 Sep 2011; revised 21 Dec 2011; accepted 4 Jan 2012; published 17 Jan 2012

VIS, Meadowlark Optics Inc., USA). The FWHM bandwidth of the tunable filter is 20 nm on average over the 400-950 nm range. The optical power at the output of the filter in each distinct spectral band, $P_{opt}(\lambda)$, centered at wavelength, λ, was determined with a calibrated photodetector. Reverse bias conditions and photocurrent measurements were carried out with a source measure unit (SMU) mainframe (HP 4142B) and each channel was referenced to the ground unit (GNDU) of the SMU. Photocurrent measurements, $I_{ph,i}$, used in the responsivity calculations were corrected for dark current offsets: $I_{ph,i} = I_i - I_{dark,i}$. Room-temperature dark current measurements for the four junctions, $I_{dark,i}$, were: 12.3 pA, 15.7 pA, 3.4 pA, 14.9 pA, respectively.

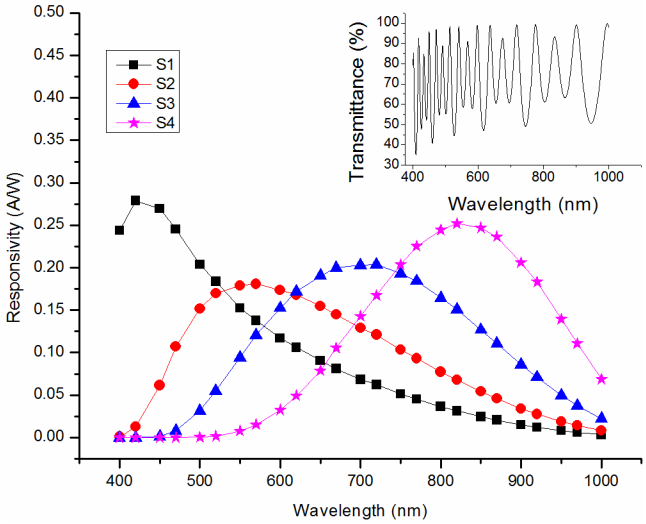

Fig. 2. Modeled spectral responses for the four individual junctions from 400 nm to 950 nm. Inset shows the modeled transmittance of the passivation layers

In addition to the native junction spectral response of the BQJ, the standard passivation layers used in the CMOS process atop the photosensitive area act as an interference filter [6], effectively modulating the transmittance of the photodetector, as shown in the inset of Fig. 2. This effect can be almost entirely eliminated using normalization, as explained below.

Figure 3 shows the experimentally-measured responsivities, $S_i(\lambda) = I_{ph,i} / P_{opt}(\lambda)$, of the BQJ photodetector in reversed bias conditions at −1.5 V for each junction, where the modulation of the responsivities due to the mutual interference from the partial reflections at the interfaces between the photodetector surface and the passivation layers is clearly visible. Note that changing bias conditions did not affect the spectral responses significantly: for reverse-bias voltages ranging from 0 to 4 V, estimations of $S_i(\lambda)$ varied by less than 5% for the surface junction and less than 1% for the buried junctions.

#155085 - $15.00 USD Received 20 Sep 2011; revised 21 Dec 2011; accepted 4 Jan 2012; published 17 Jan 2012

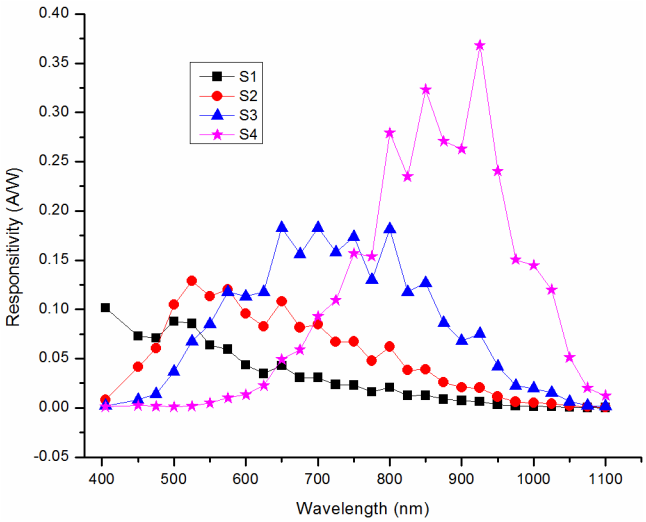

Fig. 3. Measured spectral responses of the BQJ photodetector junctions biased at −1.5 V. The modulation of the responsivities due to the mutual interference from the partial reflections at the interfaces between the photodetector surface and the passivation layers is clearly visible.

In order to compare the modeled and measured spectral responses, the wavelength-specific responsivity measurements, $S_i(\lambda)$, were normalized with respect the sum of responsivities at each wavelength:

$$N_i(\lambda) = \frac{S_i(\lambda)}{\sum_{j=1}^{4} S_j(\lambda)} = \frac{I_{ph,i}(\lambda)}{\sum_{j=1}^{4} I_{ph,j}(\lambda)}, \quad i = 1..4 \tag{2}$$

Figure 4 shows a superposition of the normalized responses, $N_i(\lambda)$, for both measured and modeled responsivities, showing good agreement between the two. This normalization suppresses the effect of the interferences of the passivation layer presents in the measured set. The small differences between the modeled and measured curves are due to the idealized cylindrical geometry of the doping profiles used in the model.

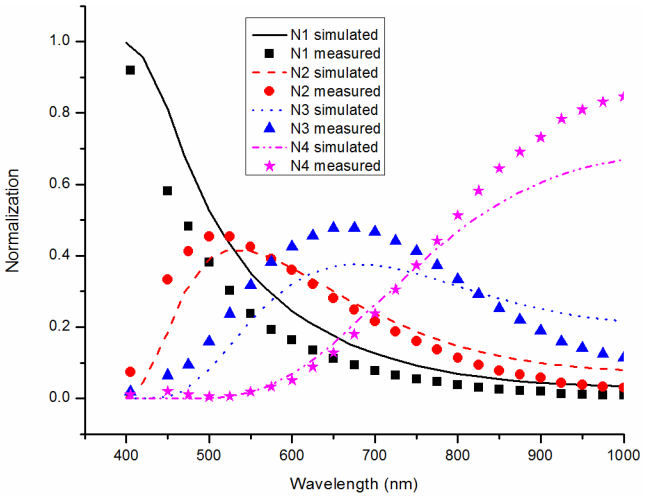

Fig. 4. Comparison of the modeled and measured normalized spectral responses, $N_i(\lambda)$.

#155085 - $15.00 USD Received 20 Sep 2011; revised 21 Dec 2011; accepted 4 Jan 2012; published 17 Jan 2012

4. Method of analysis

Using the set of responsivities, $S_i(\lambda)$, of the BQJ photodetector, an optical input with power spectrum, $\Phi(\lambda)$, is mapped to a 4-component junction photocurrent vector, I_i.

$$I_i = \int \Phi(\lambda) S_i(\lambda) d\lambda, \qquad i = 1..4 \tag{3}$$

For an optical input composed of four components, $\Phi(\lambda) = \sum_{k=1}^{4} c_k \Phi_k(\lambda)$, such as light from a mix of four fluorophores with individual power spectra, Φ_k, and modulations, c_k, Eq. (3) becomes:

$$I_i = \sum_{k=1}^{4} c_k \int \Phi_k(\lambda) S_i(\lambda) d\lambda, \qquad i = 1..4, \tag{4}$$

or

$$I_i = \sum_{k=1}^{4} c_k R_{ik}, \tag{5}$$

where

$$R_{ik} = \int \Phi_k(\lambda) S_i(\lambda) d\lambda$$

The output of the BQJ photodetector can thus be expressed with a coupled linear system of four equations:

$$\begin{bmatrix} R_{11} & R_{12} & R_{13} & R_{14} \\ R_{21} & R_{22} & R_{23} & R_{24} \\ R_{31} & R_{32} & R_{33} & R_{34} \\ R_{41} & R_{42} & R_{43} & R_{44} \end{bmatrix} \begin{bmatrix} c_1 \\ c_2 \\ c_3 \\ c_4 \end{bmatrix} = \begin{bmatrix} I_1 \\ I_2 \\ I_3 \\ I_4 \end{bmatrix} \tag{6}$$

The individual fluorophore spectra, Φ_k, are known experimental parameters and the junction responsivities, $S_i(\lambda)$, are determined a priori from the BQJ photodetector characterization (Fig. 3). Therefore, the components R_{ik} can be pre-computed. As a result, using the pre-computed matrix $\boldsymbol{R}$ with standard linear algebra techniques, the system can be solved for the particular set of modulation components, c_k, corresponding to any photocurrent measurement vector, I_i. The orthogonality of the basis functions, $S_i(\lambda)$, and resulting precision of the modulation component estimates, however, is highly dependent on the linear-independence of the junction responsivities, as discussed below.

5. Discussion and validation results

The BQJ device described here was designed for use in biochemical analysis applications using fluorescence labeling of multiple analytes, where the instrumentation is highly integrated and compact such as in labs-on-chip or miniaturized photonics-based biosensors. In advanced biochemical analysis applications, the concentration and/or kinetics of multiple analytes must be tracked in parallel. Hence, the BQJ's ability to simultaneously measure the optical power of up to four distinct spectral components is ideally suited to this task.

In practice, the ability to estimate the modulation components, c_k, in the input will closely depend on the separability of the individual components of the input spectra, Φ_k, and their

#155085 - $15.00 USD Received 20 Sep 2011; revised 21 Dec 2011; accepted 4 Jan 2012; published 17 Jan 2012

relationship to the BQJ spectral responses, $S_i(\lambda)$ (basis functions). From a linear algebra point of view, separable-component spectra that are well-matched to the BQJ spectral responses will correspond to a well-posed numerical problem, yielding good estimates of the c_k. Conversely, substantially overlapping component spectra that are poorly matched to the BQJ spectral responses will correspond to an ill-posed problem, yielding poor estimates of the c_k.

The BQJ spectral responses are set by the doping profiles and junction depths. The spectral responses are tunable to some extent to the requirements of a particular application by adjusting fabrication parameters within the ranges allowed by the HVCMOS process. Since both the p-well and p + diffusion characteristics are set by the standard low voltage CMOS process, they are not normally easily adjustable: a modification in the p-well will affect the NMOS 5V and a modification in the p + diffusion will affect the PMOS 5V. There is more tuning flexibility for the n-base and deep n-well characteristics, according the following rules: (1) the doping concentration of an embedded junction must be at least 10 times greater than the preceding junction to avoid sheet resistance instability and doping compensation; (2) the depth of an embedded junction must be at least 0.5 µm to 1 µm to prevent punch-through effects, even at low voltage.

Figure 5 shows the normalized measured responses from Fig. 4 in a way that emphasizes the relative contribution of each junction to the total spectral sensitivity, as a function of wavelength. The graph clearly illustrates that the shallow and deepest junctions (S1 & S4) have relatively distinct responses whereas the middle junctions (S2 & S3) have significantly overlapping responses.

A judicious choice of fluorophores will maximize the precision of the individual modulation component estimates, c_k, according to the following guidelines: (1) the fluorophore emitting at the shortest wavelength should have an emission spectrum centered below 450 nm; (2) the fluorophore emitting at the longest wavelength should have an emission spectrum centered in the 850-950 nm range; (3) the two remaining fluorophores should have their emission spectra in the 500 nm – 800 nm range, as distinctly separated as possible. The impact of the choice of a candidate set of fluorophores on the ability to estimate the c_k can be quantified by calculating the rank of the matrix $\boldsymbol{R}$.

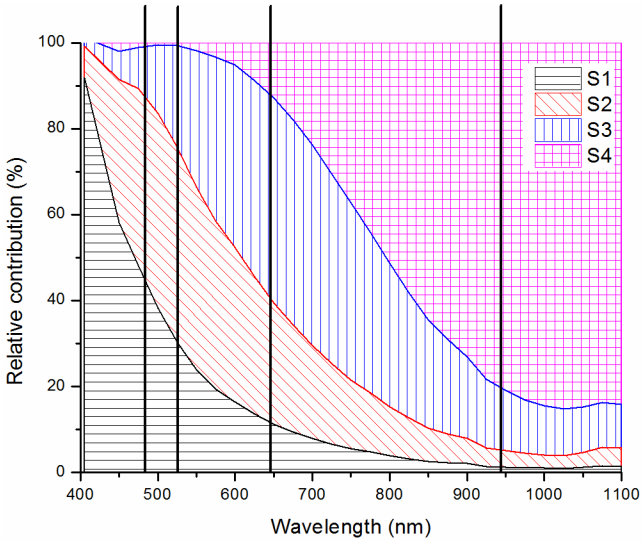

Fig. 5. Relative contribution of each junction to the total spectral sensitivity as a function of wavelength (measured set of Fig. 4). The central wavelengths of the four LEDs used in the experiment described in Fig. 6 are indicated by the vertical bars.

#155085 - $15.00 USD Received 20 Sep 2011; revised 21 Dec 2011; accepted 4 Jan 2012; published 17 Jan 2012

The performance of the BQJ device was tested using a modified version of the probe station used to estimate the spectral responses of the individual junctions (focused spot from a narrow-band swept-wavelength source illuminating the detector). This modified setup was designed to simulate the illumination arising from a combination of four fluorescent labels by replacing the swept-light source with an integrating sphere having four input ports. The input ports housed four LEDs with emission spectra centered at 470 nm, 525 nm, 650 nm, and 940 nm, respectively. The setup could thus generate a compound spectrum composed of arbitrary contributions from the four LEDs in a precisely quantifiable and repeatable manner, a result very difficult to achieve otherwise with actual fluorophores. Since the LEDs have fairly wide emission spectra, they model organic fluorophore relatively well (see Fig. 6).

The first step in the analysis method described above is to calculate the matrix components, R_{ik}. Using the modified probe station, these values can be estimated directly by selectively turning on each LED in turn and recording the photocurrents from the four junctions, effectively evaluating the integral in Eq. (5) for the sixteen components of $\boldsymbol{R}$. The rank of the matrix $\boldsymbol{R}$ constructed with such experimental measurements was typically ~4 to within two significant figures. This indicated that the system consisting of the BQJ device and the four "simulated fluorophores" (LEDs) was well-conditioned and that confidence in the estimates of the spectral modulation components was high. In an application involving actual fluorophores, calibrated test solutions of the individual fluorophores would have to be used.

A validation experiment was run with the four LEDs turned on simultaneously and the four resulting photocurrents, I_i, measured. The previously-determined matrix $\boldsymbol{R}$ was used to calculate the components, c_k, as a function of the measured photocurrents. The results of the experiment are shown in Fig. 7, along with the actual optical power outputs of the four LEDs, measured individually with a power meter (Model 1830-C + 818UV Si detector, Newport Corporation., USA). In all cases, estimated values agree to within 2% of the expected values. Additional experiments covering a range of contributions from the individual LEDs yielded similar results (not shown). Note finally that too large a discrepancy between the power levels of individual spectral components, Φ_k, will result in poor estimates overall since the bleed-through from an inordinately strong component into the spectral responses from neighboring junctions will skew results.

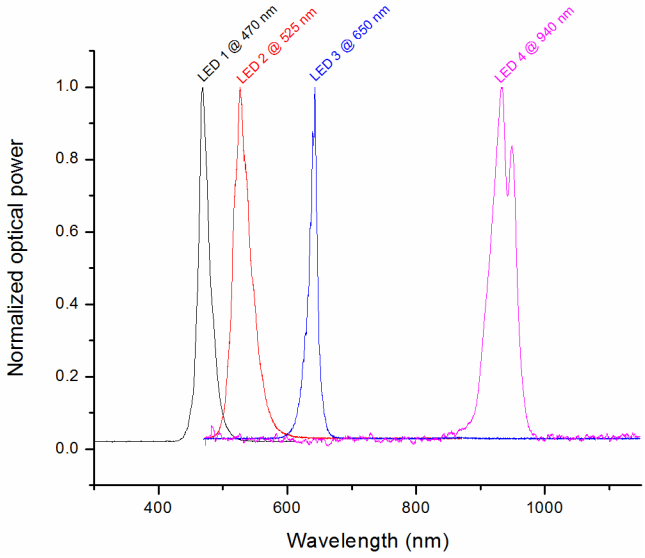

Fig. 6. Spectra of the four LEDs used in calibration and validation experiments.

#155085 - $15.00 USD Received 20 Sep 2011; revised 21 Dec 2011; accepted 4 Jan 2012; published 17 Jan 2012

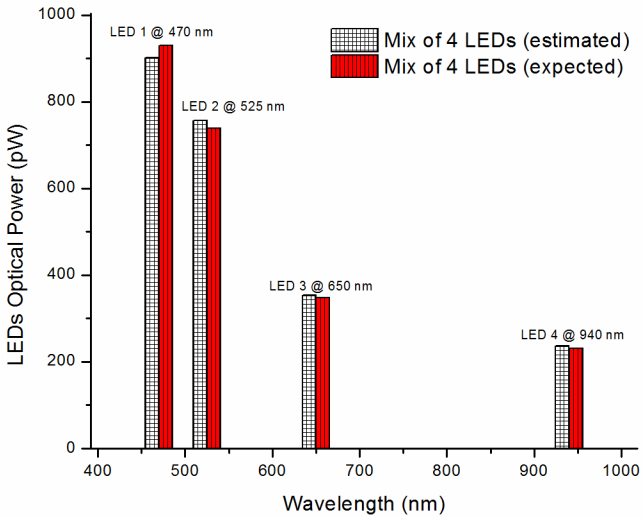

Fig. 7. Expected and estimated optical power from the four individual LEDs calculated with the matrix-based method described in the paper.

Experimental measurements were carried out on a test structure consisting of a 4×4 matrix of square pixels (pixel area: 200 μm^2, pitch: 330 µm) with a fill factor of 42%. Since the BQJ operates at relatively low voltages compared to the maximum voltage for which the HVCMOS Teledyne DALSA was designed (650V), the separation distance between pixels can be reduced further. Future design iterations will thus be capable of closer pixel spacing and higher fill ratios.

6. Conclusion

A buried quad p-n junction (BQJ) photodetector fabricated with a HV (high-voltage) CMOS process has been modeled, fabricated, and characterized. Results show that the device can be used to estimate the relative contributions of four distinct spectral components in a compound spectrum, such as that from a biochemical analysis involving the use of up to four fluorescent labels simultaneous. A judicious choice of fluorophores will maximize the precision of the individual fluorescence component estimates.

Acknowledgments

This work was supported by grants from NanoQuébec, Teledyne DALSA Semiconductor, and the Natural Sciences and Engineering Research Council of Canada (NSERC). Travel grants from the Laboratoire International Associé en Nanotechnologies et Nanosystèmes (LIA-LN2) are gratefully acknowledged.

#155085 - $15.00 USD Received 20 Sep 2011; revised 21 Dec 2011; accepted 4 Jan 2012; published 17 Jan 2012